

Optimising Event-Driven Spiking Neural Network with Regularisation and Cutoff

Dengyu Wu, Gaojie Jin, Han Yu, Xinping Yi and Xiaowei Huang

Abstract—Spiking neural network (SNN), next generation of artificial neural network (ANN) that more closely mimic natural neural networks offers promising improvements in computational efficiency. However, current SNN training methodologies predominantly employ a fixed timestep approach, overlooking the potential of dynamic inference in SNN. In this paper, we strengthen the marriage between SNN and event-driven processing with a proposal to consider cutoff in SNN, which can terminate SNN anytime during the inference to achieve efficient inference. Two novel optimisation techniques are presented to achieve inference efficient SNN: a Top-K cutoff and a regularisation. The Top-K cutoff technique optimises the inference of SNN, and the regularisation are proposed to affect the training and construct SNN with optimised performance for cutoff. We conduct an extensive set of experiments on multiple benchmark frame-based datasets, such as Cifar10/100, Tiny-ImageNet and event-based datasets, including CIFAR10-DVS, N-Caltech101 and DVS128 Gesture. The experimental results demonstrate the effectiveness of our techniques in both ANN-to-SNN conversion and direct training, affirming their compatibility and potential benefits in enhancing accuracy and reducing inference timestep when integrated with existing methods. Code available: <https://github.com/Dengyu-Wu/SNN-Regularisation-Cutoff>

Index Terms—Spiking Neural Network, Event-driven Neural Network, ANN-to-SNN Conversion, SNN Regularisation.

I. INTRODUCTION

Spiking Neural Network (SNN) has recently attracted significant research and industrial interests thanks to its energy efficiency and low latency [1], and there are neuromorphic chips such as Loihi [2] and TrueNorth [3] on which SNN can be deployed. Mechanistically, SNN mimics biological neurons, and the neurons process and forward spikes independently. With such an asynchronous working mechanism, only a (small) subset of neurons will be activated during inference. That is, computing efficiency is inherent to SNN.

The asynchronous mechanism also suggests that event-based input may make a better use of SNN. Actually, neuromorphic sensors such as Dynamic Vision Sensor [4]–[6] and Dynamic Audio Sensor (DAS) [7] have been developed to generate binary “events”, which are ideal inputs to SNN. For example, unlike conventional frame-based cameras which measure the “absolute” brightness at a constant rate, DVS

cameras are bio-inspired sensors that *asynchronously* measure per-pixel brightness changes (called “events”), and output a stream of events that encode the time, location and sign of the brightness changes [6]. DVS reveals the sparsity and asynchronicity in recognition systems for computational efficiency [8]–[10]. For frame-based input, however, an additional encoding step is imperative prior to the forward propagation in SNN [11], [12]. This process ensures that traditional visual data can be effectively processed by SNN. Irrespective of the input type—event-based or frame-based—SNN is capable of delivering sequential predictions at their outputs, showcasing they can predict at any timestep. To harness these features, we propose to consider cutoff optimal SNN, which allow the termination at any time during the inference on a spike train (i.e., an input) and return the best possible inference result. Such SNN enable the cutoff during the inference without (significantly) compromising the performance, and thus can achieve the best in terms of accuracy and latency.

Regarding the training of SNN, one approach is through ANN-to-SNN conversion, which adopts the mature training regime of ANNs to first train a high-accuracy ANN, and then convert it into SNN. Such conversions via ANNs have resulted in research to focus on achieving the near-zero conversion loss [13]–[15]. Another methodology incorporates the use of backpropagation directly in SNN training [16]–[19]. Due to the non-differentiable nature of spiking, this approach necessitates a surrogate gradient [16], [17]. In our study, we explore a novel cutoff mechanism in SNN and propose a general optimisation strategies for this process. Our ultimate goal is to develop an optimal SNN that effectively balances accuracy and latency.

This paper makes two key technical contributions. Firstly, instead of setting the inference length to always be maximum timestep T , we can explore an early cutoff mechanism that enables the SNN model to automatically achieve optimal latency and computing efficiency. As shown in Fig. 1, the SNN model will run a monitoring mechanism to determine when it is sufficiently confident to make a decision. Once such a decision is made at time $t < T$, a cutoff action is triggered so that the SNN will not take future inputs until T . Therefore, it will lead to lower latency and less computations because decision is made at time t rather than T .

The second contribution is that, we propose a regularisation technique towards improving SNN cutoff performance. This technique influences the activation distribution during ANN or SNN training, which results in an SNN that can potentially classify with less input information. As will be discussed in Method (Section IV), our proposed regulariser effectively mitigates the impact of ‘worst-case’ inputs during both ANN

D. Wu and X. Huang are with Department of Computer Science, University of Liverpool, Liverpool, United Kingdom. (E-mails: dengyu.wu@liverpool.ac.uk, xiaowei.huang@liverpool.ac.uk)

X. Yi is with National Mobile Communications Research Laboratory, Southeast University, Nanjing, China. (E-mail: xyi@seu.edu.cn)

G. Jin is with State Key Laboratory of Computer Science, Institute of Software, CAS Beijing, China. (E-mail: gaojie@ios.ac.cn)

H. Yu is with Department of Electrical Engineering, Chalmers University of Technology, Gothenburg, Sweden. (E-mail: yuha@chalmers.se)

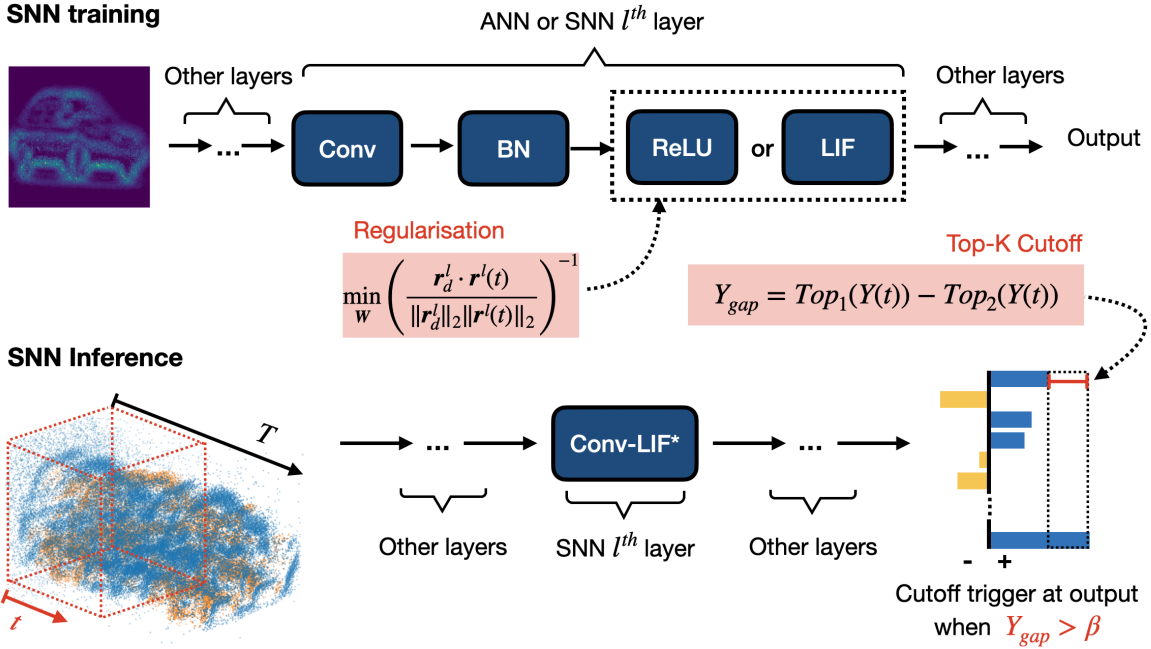


Fig. 1: An illustrative diagram showing the regularisation for optimising SNN and the cutoff mechanism for reducing latency on Cifar10-DVS dataset. Cutoff is triggered when Y_{gap} is greater than β , a value dynamically determined by a confidence rate as introduced in Section IV-A.

and SNN training phases. These worst-case samples are typically inputs that can cause failures in the early inference. Experiments in Section V-B show that we can enhance the state-of-the-art methods on both ANN-to-SNN conversion and direct training.

II. RELATED WORK

The application of SNN to a data source can be separated into two phases: training and inference. Broadly speaking, the training algorithms for SNN can be categorised into ANN-to-SNN conversion and direct training.

a) ANN-to-SNN Conversion: Early studies in ANN-to-SNN conversion, such as [20], [21], utilised the maximum activation value to normalise weights from ANNs. [11] proves that the normalisation can also be achieved by greedily searching for the optimal threshold using the input spike train. A unified conversion framework is studied in [22]. Besides, there are hybrid methods [12], [23] that combine conversion and direct training. Tandem Learning [24] leverages the gradient from ANN to update SNN during training. Recent work [13], [22] shows that, outlier elimination in ANN activations can be implemented by applying clipping operation after the Rectified Linear Unit (ReLU). Based on this, [14], [25] further minimise the quantisation error by quantisation-aware training.

b) Direct Training: In contrast to the conversion-based approach, direct training of SNN offers the capability to process temporal features effectively [19], [26]. Numerous studies focused on designing surrogate gradients [16], [17], [27], [28] to tackle the non-differentiable nature of spike generation in SNN, thereby enabling efficient backpropagation.

[26] demonstrates how the integration of temporal attention can significantly bolster SNN performance. Advancements in temporal batch normalisation [29], [30] have played a crucial role in expediting the convergence process in direct training. Furthermore, research on spiking transformers, such as in [31]–[33], offers new perspectives in this domain.

c) Adaptive Timestep in SNN: Despite these significant advancements in both ANN-to-SNN conversion and direct training, a fundamental limitation persists: the optimisation of SNN is predominantly focused on specific timestep, neglecting the potential for adaptive inference. The exploration of adaptive timestep in SNN is still in its nascent stages with limited works. Specifically, [34] introduced an additional deep network to trigger the early-exiting in SNN, a solution that may be resource-intensive for small SNN. Similarly, [35] focuses on ANN-to-SNN conversion by applying network calibration before dynamic prediction, while [36] employs conformal prediction [37] as a trigger mechanism. However, these approaches do not address the optimisation of SNN training for such adaptive timestep scenarios. Our study aims to fill this gap by combining the cutoff with a general regulariser.

III. PRELIMINARY

In this section, we discuss the event-based input in spiking neuron and introduce the ANN-to-SNN conversion. To facilitate the analysis, we use **bold symbol** to represent vector, l to denote the layer index, and i to denote the index of elements. For example, \mathbf{a}^l is a vector and a_i^l is the i -th element in \mathbf{a}^l . Inference time t represents the time length of input. \mathbf{W}^l is weight matrix at the l -th layer. T denotes the maximum

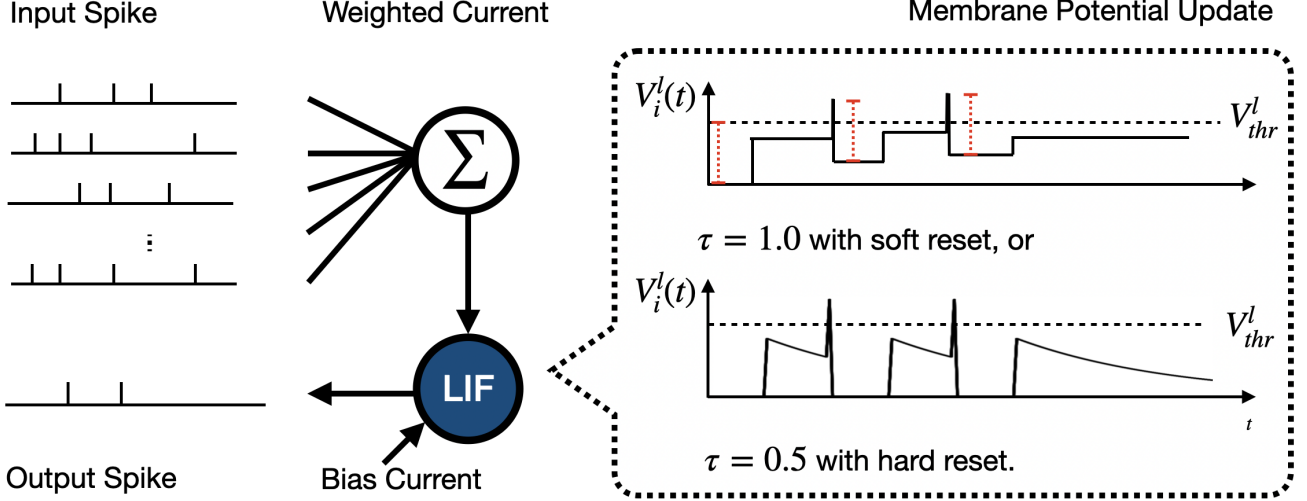


Fig. 2: Illustration of inference process in a Leaky Integrate-and-Fire (LIF) neuron within the hidden layer. During this process, the input spikes charges the membrane potential $V_i^l(t)$ through weighted and bias currents, which are learned from the training stage. When $V_i^l(t)$ reaches the threshold V_{thr}^l , the neuron will generate a spike and then reset the $V_i^l(t)$. In our study, the Integrate-and-Fire (IF) neuron with soft reset is a special case of LIF model when $\tau = 1$.

timestep and it can be various depending on dataset. T_{avg} presents the averages timestep over a set of test samples.

A. Leaky Integrate-and-Fire model

The Leaky Integrate-and-Fire (LIF) model lauded for its simplicity and its close resemblance to biological neural processing, serves as a foundational component in the study of SNN. Figure 2 shows the inference process in a single LIF neuron. The dynamic updates in the LIF neuron can be described as follows:

$$\mathbf{V}^{l-}(t) = \begin{cases} \mathbf{V}^{l+}(t-1) + \mathbf{Z}^l(t) & \text{for } l > 1, \\ \mathbf{Z}^1(t) & \text{for } l = 1. \end{cases} \quad (1)$$

where \mathbf{V}^{l-} and \mathbf{V}^{l+} denote the membrane potential before and after reset respectively. The reset process of $V_i^l(t)$ is categorised as follows:

$$V_i^{l+}(t) = \begin{cases} \tau V_i^{l-}(t)(1 - \theta_i^l(t)) & \text{for hard reset,} \\ V_i^l(t) - V_{thr}^l \theta_i^l(t) & \text{for soft reset.} \end{cases} \quad (2)$$

where $\theta^l(t)$ is a step function, i.e., $\theta_i^l(t) = 1$ if $V_i^l(t) \geq V_{thr}^l$ and $\theta_i^l(t) = 0$ otherwise. τ is decay factor and soft reset is introduced for ANN-to-SNN conversion. Specifically, conversion-based SNN inference with Integrate-and-Fire (IF) neuron with soft reset aimed at reducing the information loss caused by the conversion [14], [15], [22], [38].

In hidden layers, the weighted current $\mathbf{Z}^l(t)$ can be described as follows,

$$\mathbf{Z}^l(t) = \mathbf{W}^l \boldsymbol{\theta}^{l-1}(t) + \mathbf{b}^l \quad \text{when } l > 1. \quad (3)$$

According to different inputs, $\mathbf{Z}^l(t)$ at the first layer, i.e., $\mathbf{Z}^1(t)$, can be initialised as either

$$\text{Event-based input: } \mathbf{Z}_e^1(t) = \mathbf{W}^1 \mathbf{X}(t) + \mathbf{b}^1 \quad (4)$$

where $\mathbf{X}(t)$ is the time-dependent spike train, i.e., the input may change the charging current with time during the inference, or

$$\text{Frame-based input: } \mathbf{Z}_f^1 = \mathbf{W}^1 \bar{\mathbf{X}} + \mathbf{b}^1 \quad (5)$$

where $\bar{\mathbf{X}}$ represents the constant current based on inputs, e.g., normalised pixel value of RGB Image [14]. For each timestep, frame-based input stimulus the first layer with same level of current. Notably, for event-based input, SNN can manifest faster inference due to immediate response after receiving the first spike, and it completes the inference whenever the spike train ends, i.e., at T . The event-based benchmarks are further introduced in Section V-A. This characteristic makes it possible that the inference time is dynamic for different inputs. In this paper, with the cutoff technique as in Section IV-A, we will show that the average latency of the inference in SNN can be further reduced (to some $t \leq T$).

IV. METHODS

In Section IV-A, it presents the theoretical underpinning of cutoff mechanism for the inference. Following this, Section IV-B details the design of a general regulariser to optimise SNN regarding cutoff mechanism.

A. Cutoff mechanism in SNN

Thanks to the asynchronous working mechanism, event-driven SNN can predict when only part of the spike train is processed. Nevertheless, a naive cutoff on the length of spike train (or the sampling time of event sensor) can easily result in accuracy loss. In this section, we suggest a principled method to determine the inference time. Technically, our approach begins with a theoretical analysis of cutoff in Section IV-A1, identifying optimal cutoff timestep for each input.

More precisely, we focus on inputs that consistently allow SNN to make correct predictions in subsequent processing. The following provides the details. Then, we introduced an intermediate value in IV-A2, called confidence rate and denoted as $C(\hat{t}, D\{Y_{gap} > \beta\})$, is defined based on the statistical characteristics of processing a set D of inputs with respect to the discrete inference time \hat{t} and Y_{gap} . $Y_{gap} > \beta$ operates as a condition to identify the samples in D that are suitable for cutoff. Actually, we are able to plot a curve of confidence rate $C(\hat{t}, D\{Y_{gap} > \beta\})$ with respect to the time \hat{t} and β , respectively.

1) *Optimal Cutoff Timestep (OCT)*: To define a theoretically optimal cutoff within SNN, we propose identifying a cutoff point where subsequent predictions remain positive true. This criterion establishes the cutoff as the minimal necessary duration of input processing required to uphold predictive reliability. Thus, we write $\mathbf{X}[\hat{t}] = \sum_{t=0}^{\hat{t}} \mathbf{X}(t)$ to denote the accumulation of $\mathbf{X}(t)$ from 0 up to \hat{t} . Then, we let $f(\mathbf{X}[\hat{t}])$ return the prediction of f based on the partial input $\mathbf{X}[\hat{t}]$. Based on this, we define the Optimal Cutoff Timestep (OCT) as

$$g(\mathbf{X}) = \arg \min_{\hat{t}} \{\forall \hat{t}_1 > \hat{t} : \mathbf{1}(f(\mathbf{X}[\hat{t}_1]) = \mathbf{y})\} \quad (6)$$

to express the earliest time from which the model f is able to confidently and correctly classify according to the partial input. $\mathbf{1}(\cdot)$ is the indicator function, i.e., $\mathbf{1}(x_1 = x_2) = 1$ and $\mathbf{1}(x_1 \neq x_2) = 0$. $\mathbf{1}(f(\mathbf{X}[\hat{t}_1]) = \mathbf{y})$ suggests that $f(\mathbf{X}[\hat{t}_1])$ is the same as the ground truth \mathbf{y} . The function $g(\mathbf{X})$ represents a theoretical lower bound of average inference timestep, ensuring that each input sample can undergo minimal inference timestep without sacrificing accuracy.

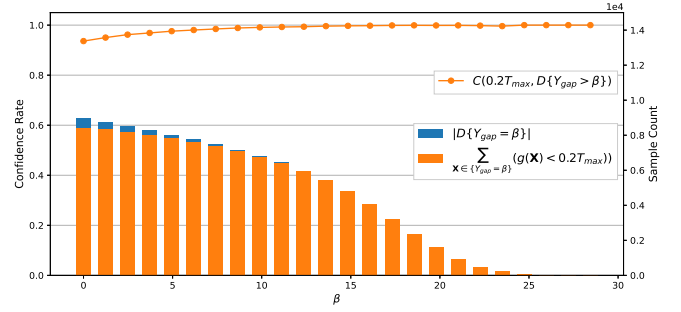
In our evaluations, we will utilise the OCT as a novel metric to assess the performance of SNN models in terms of their cutoff efficiency. This metric will enable us to quantitatively determine the lower boundary of the cutoff for any given sample, pinpointing the earliest timestep at which our SNN models can deliver reliable predictions.

2) *Top-K Gap for Cutoff Approximation*: During runtime inference, a critical challenge emerges due to the unpredictability of future predictions, which makes determining the OCT in real time unfeasible. To tackle this, we introduce a cutoff mechanism based on the gap between the top-1 and top-2 output predictions. This ‘Top-K’ approach posits that a large gap between in between these two output value implies little possibility of switching the prediction results during inference, thereby signaling an appropriate point for cutoff. To formalize this concept, we define $Top_k(\mathbf{Y}(t))$ as the top- k output occurring in one neuron of output layer. We then introduce the variable

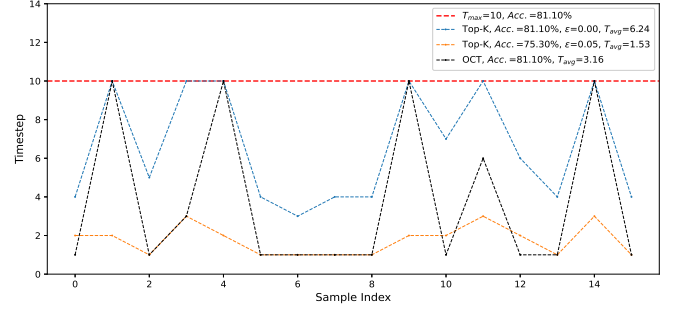
$$Y_{gap} = Top_1(\mathbf{Y}(t)) - Top_2(\mathbf{Y}(t)), \quad (7)$$

which denotes the gap of top-1 and top-2 values of output $\mathbf{Y}(t)$. Then, we let $D\{\cdot\}$ denote the inputs in subset of D that satisfy a certain condition. Now, we can define the confidence rate as follows:

$$\text{Confidence rate: } C(\hat{t}, D\{Y_{gap} > \beta\}) = \frac{1}{|D\{Y_{gap} > \beta\}|} \sum_{\mathbf{X} \in D\{Y_{gap} > \beta\}} (g(\mathbf{X}) \leq \hat{t}), \quad (8)$$



(a) Confidence w.r.t β at $0.2 T$



(b) Timestep w.r.t sample index.

Fig. 3: Evaluation of the Top-K cutoff on Cifar10-DVS, using a directly trained SNN model with $T = 10$ (as detailed in Section V). (a) presents the increase of β will limit the number of samples eligible for cutoff, while concurrently enhancing the confidence in the cutoff decision. For enhanced readability, (b) shows the inference timestep of 16 samples from test dataset under varied trigger conditions.

which intuitively computes the percentage of inputs in D that can achieve the prediction success at or before T , i.e., $g(\mathbf{X}) \leq \hat{t}$. $|D\{Y_{gap} > \beta\}|$ denotes the number of samples in D satisfying the condition. It is not hard to see that, when $\hat{t} = 0$, $C(\hat{t}, D\{Y_{gap} > \beta\})$ is also 0, and with the increase of time \hat{t} , $C(\hat{t}, D\{Y_{gap} > \beta\})$ will also increase until reaching 1. Our algorithm searches for a minimum $\beta \in \mathbb{R}^+$ at a specific \hat{t} , as expressed in the following optimisation objective:

$$\arg \min_{\beta} C(\hat{t}, D\{Y_{gap} > \beta\}) \geq 1 - \epsilon, \quad (9)$$

where ϵ is a pre-specified constant such that $1 - \epsilon$ represents an acceptable level of confidence for activating cutoff, and a set of β is extracted under different \hat{t} using training samples.

Fig. 3 provides a visual representation of Equations 6 to 9, illustrating the theoretical concepts in a comprehensive manner. Additionally, Fig. 3b highlights the performance disparity between OCT and Top-K cutoff. The OCT provides a theoretically minimum timestep of each sample, ensuring the prediction of the sample maintains correct as if processed for the full duration, T . Adjusting the ϵ parameter in the Top-K cutoff allows for reduced average timestep but may lead to a compromise in accuracy. This insight directs our primary optimisation goal towards enhancing SNN cutoff performance, a significant departure from traditional SNN optimisations [14], [18], [19], [26], [39] that typically emphasise a fixed timestep approach.

B. Optimising SNN for Cutoff

To improve the cutoff performance, we concentrate on improving the cosine similarity between the actual spiking rate at time t , $\mathbf{r}^l(t)$, and the desired spiking rate, $\tilde{\mathbf{r}}^l$. This approach ensures that our regularisation technique can be effectively integrated with eight ANN-to-SNN conversion or direct training, contributing to enhanced performance. Our objective can be formulated as follows:

$$\min_{\mathbf{W}} \left(\frac{\tilde{\mathbf{r}}^l \cdot \mathbf{r}^l(t)}{\|\tilde{\mathbf{r}}^l\|_2 \|\mathbf{r}^l(t)\|_2} \right)^{-1}, \quad (10)$$

where $\tilde{\mathbf{r}}^l$ is desired spiking rate and $\mathbf{r}^l(t)$ denotes the spiking rate at time t . Both of them will be approximated differently according to conversion (Section IV-B1) and direct training (Section IV-B2).

Actually, [40] showed that the cosine similarity between full precision and quantised neural network has a high correlation with the final accuracy of the quantised neural network. Similarly, we expect that higher cosine similarity between $\tilde{\mathbf{r}}^l$ and $\mathbf{r}^l(t)$ can result in less accuracy drop by t . As we proceed, one of the main challenges we face is approximating these two spiking rates, particularly within the framework of ANN-to-SNN conversion and direct training.

To clearly differentiate, in the rest analysis, we will $\tilde{\mathbf{r}}_c^l$ and $\mathbf{r}_c^l(t)$ to denote the desired spiking rate and spiking rate at time t , respectively, in the conversion-based method, and $\tilde{\mathbf{r}}_d^l$ and $\mathbf{r}_d^l(t)$ in direct training. Each method necessitates a distinct approach to approximate these rates, reflecting their unique operational contexts. It is important to note that there is no established evidence suggesting that Equation 10 directly optimises accuracy at T . Consequently, to prevent any potential degradation of the original training performance, our approach with the Regulariser of Cosine Similarity (RCS) only focuses those samples that yield correct predictions at T .

1) *Regularising ANN before conversion*: For conversion-based SNN, [20], [22] introduced on a fundamental relationship between spiking rates $\mathbf{r}^l(t)$ and ReLU activation \mathbf{a}^l , which gives:

$$\mathbf{r}_c^l(t) = \frac{1}{V_{thr}^l} \left(\mathbf{W}^l \mathbf{r}_c^{l-1}(t) + \mathbf{b}^l \right) - \Delta^l(t), \quad (11)$$

where $\mathbf{r}_c^l(t) = \frac{1}{t} \sum^{t'} \theta^l(t')$ denotes the spiking rate at time t , with t' representing each discrete timestep leading up to t at the l -th layer, and $\Delta^l(t) \triangleq \mathbf{V}^l(t)/(tV_{thr}^l)$ represents the residual spiking rate.

The spiking rate at the first layer can be initialised as $\mathbf{r}_c^1(t) = \mathbf{a}^1/V_{thr}^1 - \Delta^1(t)$. when t is sufficiently large to make $\Delta^l(t)$ negligible, we have the desired spiking rate for the l -th layer as follows:

$$\tilde{\mathbf{r}}_c^l = \mathbf{a}^l/V_{thr}^l \quad (12)$$

Given that $\mathbf{r}_c^l(t) = \tilde{\mathbf{r}}_c^l - \Delta^l(t)$, we can express the cosine similarity as follows:

Algorithm 1 Compute RCS loss in ANN training

Require: Dataset \mathcal{D} , ANN prediction function $f_{ann}(\cdot)$, L layer number, batch size B

- 1: **for** each batch \mathcal{B} in \mathcal{D} of size B **do**
 - 2: Initialize \mathbf{A}_{batch}^l to store activations for layer l
 - 3: Initialize \mathbf{A}_{norm}^l to store L2 norms for layer l
 - 4: **for** each data point $(\bar{\mathbf{X}}, y)$ in \mathcal{B} **do**
 - 5: Compute prediction: $\hat{y} = f_{ann}(\bar{\mathbf{X}})$
 - 6: **if** \hat{y} is correct **then**
 - 7: Append layer l activations \mathbf{a}^l to \mathbf{A}_{batch}^l
 - 8: **end if**
 - 9: **end for**
 - 10: Compute A_{max} as the maximum value in \mathbf{A}_{batch}^l
 - 11: **for** each \mathbf{a}^l in \mathbf{A}_{batch}^l **do**
 - 12: Append $\|\mathbf{a}^l\|_2$ to \mathbf{A}_{norm}^l
 - 13: **end for**
 - 14: Compute A_{min} as the minimum value in \mathbf{A}_{norm}^l
 - 15: $L_{rCS} \leftarrow \frac{1}{L} \sum_l \sqrt{n^l \frac{A_{max}^l}{A_{min}^l}}$
 - 16: **end for**
-

$$\begin{aligned} \frac{\tilde{\mathbf{r}}_c^l \cdot \mathbf{r}_c^l(t)}{\|\tilde{\mathbf{r}}_c^l\|_2 \|\mathbf{r}_c^l(t)\|_2} &\geq \frac{\|\tilde{\mathbf{r}}_c^l\|_2}{\|\tilde{\mathbf{r}}_c^l\|_2 + \|\Delta^l(t)\|_2} \\ &= \frac{\|\mathbf{a}^l\|_2}{\|\mathbf{a}^l\|_2 + \|\mathbf{V}^l(t)/(t)\|_2} \end{aligned} \quad (13)$$

Assuming that elements in $\mathbf{V}^l(t)$ satisfy uniform distribution over the time t and they are in $[0, V_{thr}^l]$, we can derive $\mathbb{E}(\|\mathbf{V}(t)/(tS_r)\|_2) \leq \sqrt{n^l V_{thr}^l}/(\sqrt{3}tS_r)$ (proof in Appendix A) Moreover, at high dimensions, the relative error made as considering $\mathbb{E}(\|\mathbf{V}(t)/t\|_2)$ instead of the random variable $\|\mathbf{V}(t)/t\|_2$ becomes asymptotically negligible [40], [41]. Therefore, the lower bound of Equation 13 can be computed as following:

$$\begin{aligned} \frac{\tilde{\mathbf{r}}_c^l \cdot \mathbf{r}_c^l(t)}{\|\tilde{\mathbf{r}}_c^l\|_2 \|\mathbf{r}_c^l(t)\|_2} &\geq \frac{\|\mathbf{a}^l\|_2}{\|\mathbf{a}^l\|_2 + \sqrt{n^l V_{thr}^l}/(\sqrt{3}t)} \\ &= \frac{\sqrt{3}t}{\sqrt{3}t + \sqrt{n^l V_{thr}^l}/\|\mathbf{a}^l\|_2} \end{aligned} \quad (14)$$

which explicitly explains that (1) the increase of t to $t \gg \sqrt{n^l V_{thr}^l}/\|\mathbf{a}^l\|_2$ can increase the lower bound and (2) it is possible to minimise term $\sqrt{n^l V_{thr}^l}/\|\mathbf{a}^l\|_2$ for developing an SNN with optimised performance at any time during the inference. In other words, for a conversion-based SNN to achieve optimal cutoff performance, the model expects a good (small) ratio of threshold voltage V_{thr}^l to average accumulated current, i.e., $\|\mathbf{a}^l\|_2/\sqrt{n^l}$, while not degrading SNN classification performance.

In ANN training, our aim is to affect the training process to results SNN for optimal cutoff. For this, Algorithm 1 has been designed to increase the lower bound defined in Equation 14. Following [20], [22], we use the maximum activation value, denoted as A_{max} in the algorithm, to approximate the threshold voltage V_{thr}^l at each layer. The algorithm works

by optimising the activation ratios within each layer during training, directly contributing to improved SNN performance.

2) *Regularising Direct Training*: In the case of direct training, SNN indicates their potential at processing spatio-temporal data, leading to a dynamic spiking rate $r_d^l(t)$ throughout the inference process. This capability highlighted in [26], sets them apart from conversion-based SNN, which are primarily designed for static input processing. To approximate the spiking rate in such training, we consider the following formulation:

$$r_d^l(t) = \theta^l(t) + \mathbf{V}^{l+}(t)/V_{thr}^l. \quad (15)$$

where $\theta^l(t)$ is generated spikes and the normalised residual membrane potential $\mathbf{V}^{l+}(t)/V_{thr}^l$ reflects the firing intention of neurons.

Moving on to the next step, we turn our attention to computing the desired spiking rate \tilde{r}_d . The trend that SNN accuracy improves with an increased number of timestep, attributed to the accumulation of relevant information over time, is illustrated by Figure 4 in Section V. This observation forms the basis for our estimation of \tilde{r}_d , which is calculated as follows:

$$\tilde{r}_d = \frac{1}{N} \sum_{t=T-N}^T r_d^l(t), \quad (16)$$

where N is an integer hyperparameter. This method posits that the later spiking rates could serve as a more representative information for a given sample. As indicated in Equation 6 from Section IV-A1, consistent and correct predictions are crucial for optimal cutoff performance. Thus, we only optimise $r_d(t)$ using Equation 10 only when the last N predictions are correct. The details of this approach are described in Algorithm 2.

V. EXPERIMENT

In this section, we engage in comprehensive experiments to evaluate SNN models using our newly proposed metric ‘OCT’, in conjunction with the ‘Top-K’ cutoff and the ‘RCS’ regularisation technique. These experiments are designed to explore the compatibility of our approaches with prevalent SNN training methods. For example, in the conversion-based training, we implement the Quantised Clip-Floor-Shift (QCFS) method from [14]. This method replaces ReLU by QCFS activation function to reduce the accuracy loss after conversion. For direct training, we adopt the Temporal Efficient Training (TET) [39] and Temporal Efficient Batch Normalisation (TEBN) [30], both representing the most recent developments in SNN training algorithms. For clarity, each the configuration in our experimental setup is denoted within brackets: QCFS(\cdot) indicates the quantisation length, while TET(\cdot) and TEBN(\cdot) refer to the pre-configured timestep. Additionally, Top-K(\cdot) indicates the setting of ϵ . In addition to these specific training methods, our experiments also incorporate a hyper-parameter α to balance the regularisation loss L_{rcs} from Algorithms 1 and 2 against the original loss function. For an easy reference to the incorporated techniques in the models, we use notations such as ‘TET(\cdot) + RCS, w/ Top-K’, indicating that the SNN

Algorithm 2 Compute RCS loss in SNN training

Require: Dataset \mathcal{D} , SNN prediction function $f_{snn}(\cdot)$, L layer number, batch size B

```

1: for each batch  $\mathcal{B}$  in  $\mathcal{D}$  of size  $B$  do
2:   Initialize  $\mathbf{S}_{batch}^l$  to store cosine similarity for the layer  $l$ 
3:   for each data point  $(\mathbf{X}, y)$  in  $\mathcal{B}$  do
4:     Set  $consistent\_correct = \text{True}$ 
5:     for  $t = T - N$  to  $T$  do
6:       Compute prediction:  $\hat{y} = f_{snn}(\mathbf{X}, t)$ 
7:       if  $\hat{y}$  is not correct then
8:         Set  $consistent\_correct = \text{False}$ 
9:       end if
10:    end for
11:    if  $consistent\_correct$  is True then
12:      for each layer  $l$  do
13:        Compute  $\tilde{r}_d = \frac{1}{N} \sum_{t=T-N}^T r_d^l(t)$ 
14:        Compute  $\frac{1}{T} \sum_t \frac{\tilde{r}_d \cdot r_d^l(t)}{\|\tilde{r}_d\|_2 \|r_d^l(t)\|_2}$ 
           and append to  $\mathbf{S}_{batch}^l$ 
15:      end for
16:    end if
17:  end for
18:  for each layer  $l$  do
19:    Compute  $\mathbf{S}_{min}^l$  as the minimum value in  $\mathbf{S}_{batch}^l$ 
20:     $L_{rcs} \leftarrow \frac{1}{L} \sum_l (\mathbf{S}_{min}^l)^{-1}$ 
21:  end for
22: end for

```

model has been enhanced with both RCS regularisation and the Top-K cutoff strategy. In our experiments, the ANN-to-SNN conversion method, such as QCFS, is applied only to frame-based datasets. We do not evaluate it on event-based datasets, which inherently involve temporal dynamics, as it primarily focuses on spatial information.

A. Experimental Datasets and Setup

The experiments are conducted across a variety of datasets, including both frame-based and event-based inputs, and network architectures. Specifically, we evaluate our approaches across diverse settings: ResNet-18 [42] for Cifar10/100 [43] and Tiny-ImageNet [44], VGGsNN [39] for Cifar10-DVS [45] and N-Caltech101 [46], along with a 5-layer convolutional network [19] for DVS128 Gesture [8]. To effectively process event-based datasets, we implement a downsampling strategy by integrating a 4×4 kernel with a stride of 4 at the beginning of the original network architecture. This adjustment can the directly feed event data into the SNN, as suggested by [47].

The samples in the event-based datasets record the event addresses with on/off events over a period of time. For Cifar10-DVS, it consists of 10,000 samples extracted from Cifar10 [45]. Each sample has 128×128 spatial resolution. The length of each spike train is less equal to 1.3s. For N-Caltech101, it has 8709 samples categorised into 101 classes. The number of samples in each class ranges from 31 to 800. The length of each spike train is about 0.3s. The width in x-direction does not exceed 240 pixels and in y-direction does

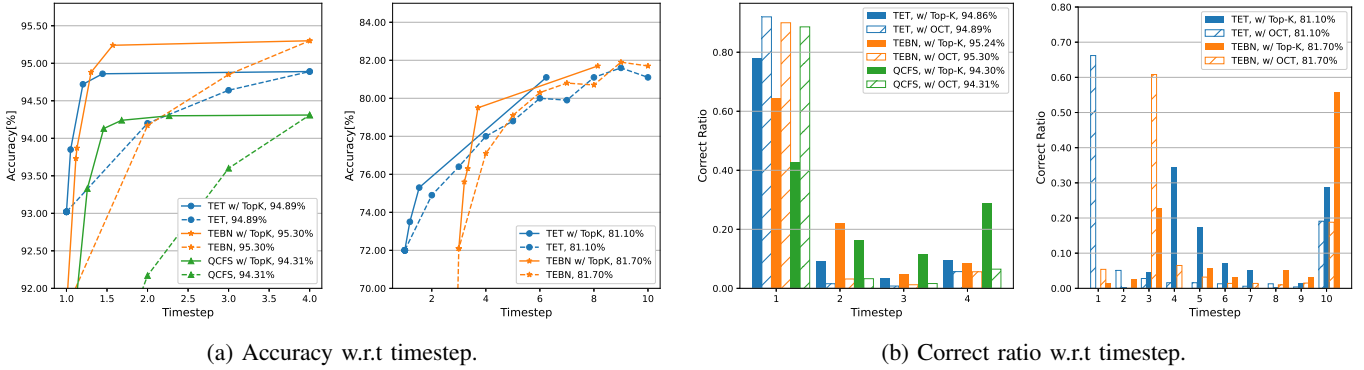


Fig. 4: Comparison of the Top-K cutoff on Cifar10 (left) and Cifar10-DVS (right) across various training methods. (a) Top-K cutoff determined by ϵ values ranging from 0.00 to 0.50 in increments of 0.05. (b) The statistic data is extracted from testing samples under $\epsilon = 0.02$ for Cifar10 $\epsilon = 0.0$ for Cifar10-DVS.

not exceed 180 pixels. For this two datasets, we use 90% samples in each class for training and 10% for testing. DVS128 Gesture consists of 1341 samples with 11 categories. Each sample is repetitive over 6.0s. Due to the repetitive information in these samples, we select the first 1.3s. All event-based samples are split into 10 frames for the training and evaluation.

For training, the hyper-parameter α varied depending on the training method and dataset, chosen from 0.001, 0.002, 0.003 for conversion-based methods and 0.001, 0.003, 0.005 for event-based datasets. For frame-based datasets like Cifar10/100 and Tiny-ImageNet, we used a batch size of 128 and 300 epochs. The auto augmentation [48] is deployed for Cifar10/100 for accuracy enhancement. For event-based datasets, training parameters were adjusted to 100 epochs with batch sizes of 128 for Cifar10-DVS, 64 for N-Caltech101, and 32 for DVS128 Gesture.

In the evaluation of Top-K cutoff, characterising the model requires a set of β values derived from the training dataset. Given that models often exhibit overconfidence post-training, we integrated dropout layers, with a dropout rate of 0.3, after each spiking layer to counteract this effect during the characterisation process. The efficacy of this dropout intervention and its impact can be further understood through the findings in [49], [50].

B. Experimental results

Figure 4 demonstrates the implementation of the Top-K cutoff across various SNN training methods, illustrating its capability to achieve computing efficiency by propagating with fewer timestep to achieve comparable accuracy. This is contrasted with the performance of original methods inference with specific timestep, where reducing these timestep often results in considerable accuracy loss. The Top-K cutoff thus proves its worth in preserving performance across different SNN models. However, it is important to note that while Top-K serves as a practical approximation, a discernible gap still exists between this empirical approach and the theoretical ideals set by our OCT metric. Specifically, the OCT suggests that a greater number of samples could potentially achieve correct predictions at the early timestep, a prospect not fully

realised by the empirical approach of the Top-K cutoff. This figure not only underscores the practical benefits of Top-K but also draws attention to the remaining differences between empirical and theoretical cutoffs in SNN inference. To provide further insight, we revisit Figure 3 from Section IV-A2, which, based on the TET(10) model, visually illustrates the impact of different ϵ values on performance across different samples.

Given that RCS is tailored to complement the OCT, our experimental results consider the OCT as a key metric associated with Top-K on frame-based inputs (Table I) and event-based inputs (II). When RCS is applied, a decrease in OCT for the same input suggests the improved accuracy of an SNN model at the early timestep. This is evident in conversion-based models in Table I. For instance, RCS facilitates a significant OCT reduction for the QCFS models, ranging from 0.01 to 0.03 across Cifar10/100 and Tiny-ImageNet. Particularly on Cifar100, this improvement manifests as a 0.3 decrease in OCT alongside a 1.01% boost in accuracy, underlining the effectiveness of RCS in enhancing SNN from ANN training. Conversely, when RCS is applied to direct training methods like TET and TEbn, the improvements on frame-based datasets appear more modest. This phenomenon may be attributed to the already small timestep utilised in these methods, which limits the the capacity of networks for representation. However, the benefits of RCS become more evident with event-based inputs, as seen in Table II. RCS facilitates a significant reduction in OCT for these inputs, with reductions ranging from 0.02 to 0.52.

Moreover, Figure 5 illustrates the impact of RCS on Top-K cutoff accuracy. Notably, the implementation of RCS shifts the accuracy curve upward compared to the curve without RCS, which means that same accuracy can have less inference time for same inputs. The exploration of cutoff in SNN reveals a clear demarcation between adaptive and traditional fixed timestep approaches in the field. Our study considers adaptive mechanisms in the SNN training stage. Unlike the reliance on auxiliary networks [34], our approaches preserve the inherent structure of the SNN architecture, optimising it intrinsically and enhancing its performance through a straightforward cut-off trigger.

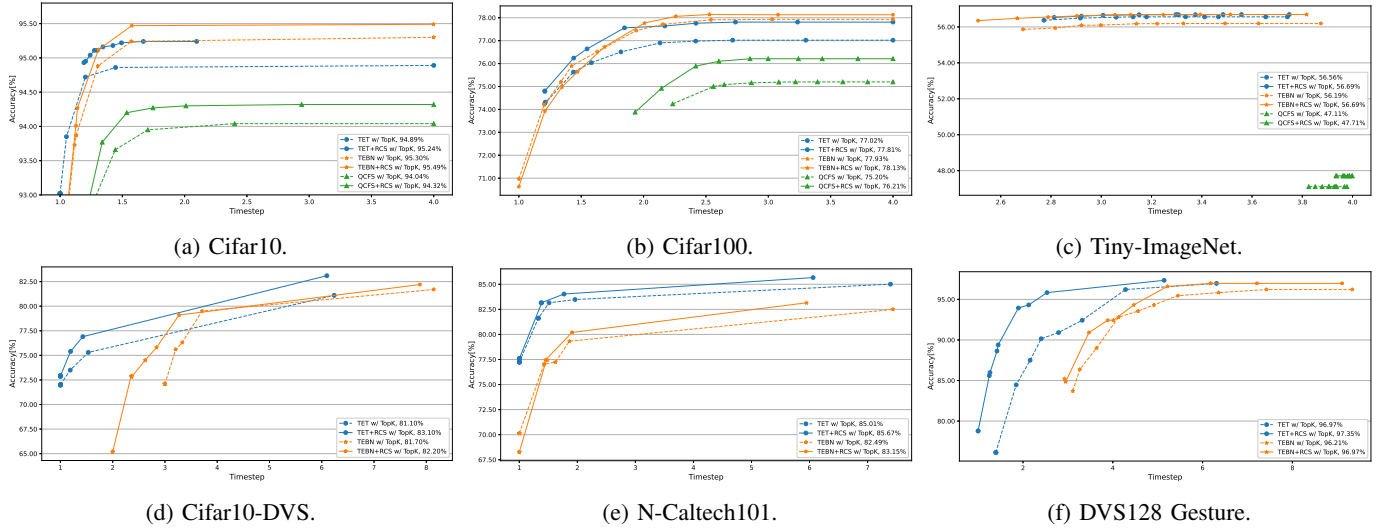


Fig. 5: Comparison of Top-K cutoff accuracy before (dashed lines) and after (solid lines) regularisation, across a range of ϵ values from 0.00 to 0.50, increasing in steps of 0.05. The accuracy for full-length input is detailed in the legend.

TABLE I: Comparison of SNN model performance on frame-based dataset using ANN-to-SNN conversion and direct training methods, with all models operating at a maximum timestep of 4. OCT reflects the theoretical cutoff performance, showcasing undiminished accuracy and the average optimal cutoff timestep. Top-K cutoff with ϵ values of 0.0 and 0.05 demonstrates the impact of approximated cutoff.

Models	OCT		Top-K(0)		Top-K(0.05)	
	Acc.	T_{avg}	Acc.	T_{avg}	Acc.	T_{avg}
QCFS(4)	94.04	1.27	94.04	4.00	94.04	2.40
QCFS(4) + RCS	94.32	1.26	94.32	4.00	94.32	2.94
TET(4)	94.89	1.20	94.89	4.00	94.86	1.45
TET(4) + RCS	95.24	1.19	95.24	2.10	95.23	1.67
TEBN(4)	95.30	1.22	95.30	4.00	95.24	1.57
TEBN(4) + RCS	95.49	1.22	95.49	4.00	95.47	1.58

(a) Accuracy and average timestep on Cifar10.

Models	OCT		Top-K(0)		Top-K(0.05)	
	Acc.	T_{avg}	Acc.	T_{avg}	Acc.	T_{avg}
QCFS(4)	75.20	2.03	75.20	4.00	75.20	3.80
QCFS(4) + RCS	76.21	2.00	76.21	4.00	76.21	3.72
TET(4)	77.02	1.84	77.02	4.00	77.02	3.30
TET(4) + RCS	77.81	1.81	77.81	4.00	77.81	3.23
TEBN(4)	77.93	1.85	77.93	4.00	77.93	3.03
TEBN(4) + RCS	78.13	1.85	78.13	4.00	78.13	3.08

(b) Accuracy and average timestep on Cifar100.

Models	OCT		Top-K(0)		Top-K(0.05)	
	Acc.	T_{avg}	Acc.	T_{avg}	Acc.	T_{avg}
QCFS(4)	47.11	2.97	47.11	3.98	47.11	3.91
QCFS(4) + RCS	47.71	2.94	47.71	3.99	47.71	3.97
TET(4)	56.56	2.52	56.56	3.74	56.56	3.65
TET(4) + RCS	56.69	2.52	56.69	3.75	56.69	3.56
TEBN(4)	56.19	2.56	56.19	3.87	56.19	3.63
TEBN(4) + RCS	56.69	2.54	56.69	3.82	56.69	3.51

(c) Accuracy and average timestep on Tiny-ImageNet.

TABLE II: Comparison of SNN model performance on event-based dataset using direct training methods, with all models operating at a maximum timestep of 10.

Models	OCT		Top-K(0)		Top-K(0.05)	
	Acc.	T_{avg}	Acc.	T_{avg}	Acc.	T_{avg}
TET(10)	81.10	3.16	81.10	6.24	75.30	1.53
TET(10) + RCS	83.10	3.05	83.10	6.10	76.90	1.43
TEBN(10)	81.70	4.46	81.70	8.14	79.95	3.71
TEBN(10) + RCS	82.20	3.94	82.20	7.88	79.10	3.27

(a) Accuracy and average timestep on Cifar10-DVS.

Models	OCT		Top-K(0)		Top-K(0.05)	
	Acc.	T_{avg}	Acc.	T_{avg}	Acc.	T_{avg}
TET(10)	85.01	2.64	85.01	7.39	83.48	1.96
TET(10) + RCS	85.66	2.57	85.67	6.06	84.03	1.77
TEBN(10)	82.49	3.01	82.49	7.44	79.32	1.86
TEBN(10) + RCS	83.15	2.99	83.15	5.95	80.20	1.91

(b) Accuracy and average timestep on N-Caltech101.

Models	OCT		Top-K(0)		Top-K(0.05)	
	Acc.	T_{avg}	Acc.	T_{avg}	Acc.	T_{avg}
TET(10)	96.97	2.18	96.97	6.31	96.21	4.28
TET(10) + RCS	97.35	1.66	97.35	5.14	95.83	2.53
TEBN(10)	96.21	3.00	96.21	9.3	96.21	7.42
TEBN(10) + RCS	96.97	2.73	96.97	9.1	96.97	7.21

(c) Accuracy and average timestep on DVS128 Gesture.

VI. CONCLUSIONS

In this paper, we focus on the development of SNN that achieve high efficiency throughout both training and inference process, making them particularly well-suited for inferring with adaptive timestep. We introduce two key innovations designed to enhance SNN performance: a regulariser targets the training phase, and a cutoff mechanism optimises the inference stage. Our comprehensive experiments showcase these advancements, marking notable enhancements in accuracy and inference efficiency over traditional methods. The Top-K cutoff technique introduced here is designed with hardware

considerations in mind and proves to be versatile across various SNN neuron models, such as IF and LIF, provided the predictions rely solely on output analysis.

REFERENCES

- [1] M. Pfeiffer and T. Pfeil, "Deep learning with spiking neurons: Opportunities and challenges," *Frontiers in Neuroscience*, vol. 12, p. 774, 2018.
- [2] M. Davies, N. Srinivasa, T.-H. Lin, G. Chinya, Y. Cao, S. H. Choday, G. Dimou, P. Joshi, N. Imam, S. Jain, *et al.*, "Loihi: A neuromorphic manycore processor with on-chip learning," *IEEE Micro*, vol. 38, no. 1, pp. 82–99, 2018.
- [3] F. Akopyan, J. Sawada, A. Cassidy, R. Alvarez-Icaza, J. Arthur, P. Merolla, N. Imam, Y. Nakamura, P. Datta, G.-J. Nam, *et al.*, "Truenorth: Design and tool flow of a 65 mw 1 million neuron programmable neurosynaptic chip," *IEEE transactions on computer-aided design of integrated circuits and systems*, vol. 34, no. 10, pp. 1537–1557, 2015.
- [4] P. Lichtsteiner, C. Posch, and T. Delbruck, "A 128×128 120 db $15\mu\text{s}$ latency asynchronous temporal contrast vision sensor," *IEEE journal of solid-state circuits*, vol. 43, no. 2, pp. 566–576, 2008.
- [5] T. Delbrück, B. Linares-Barranco, E. Culurciello, and C. Posch, "Activity-driven, event-based vision sensors," in *Proceedings of 2010 IEEE International Symposium on Circuits and Systems*. IEEE, 2010, pp. 2426–2429.
- [6] G. Gallego, T. Delbrück, G. Orchard, C. Bartolozzi, B. Tabá, A. Censi, S. Leutenegger, A. J. Davison, J. Conradt, K. Daniilidis, *et al.*, "Event-based vision: A survey," *IEEE transactions on pattern analysis and machine intelligence*, vol. 44, no. 1, pp. 154–180, 2020.
- [7] J. Anumula, D. Neil, T. Delbruck, and S.-C. Liu, "Feature representations for neuromorphic audio spike streams," *Frontiers in Neuroscience*, vol. 12, p. 23, 2018.
- [8] A. Amir, B. Tabá, D. Berg, T. Melano, J. McKinstry, C. Di Nolfo, T. Nayak, A. Andreopoulos, G. Garreau, M. Mendoza, *et al.*, "A low power, fully event-based gesture recognition system," in *Proceedings of the IEEE Conference on Computer Vision and Pattern Recognition*, 2017, pp. 7243–7252.
- [9] N. Messikommer, D. Gehrig, A. Loquercio, and D. Scaramuzza, "Event-based asynchronous sparse convolutional networks," in *European Conference on Computer Vision*. Springer, 2020, pp. 415–431.
- [10] J. Kim, J. Bae, G. Park, D. Zhang, and Y. M. Kim, "N-imagenet: Towards robust, fine-grained object recognition with event cameras," in *Proceedings of the IEEE/CVF International Conference on Computer Vision*, 2021, pp. 2146–2156.
- [11] A. Sengupta, Y. Ye, R. Wang, C. Liu, and K. Roy, "Going deeper in spiking neural networks: VGG and residual architectures," *Frontiers in Neuroscience*, vol. 13, p. 95, 2019.
- [12] N. Rathi and K. Roy, "DIET-SNN: A low-latency spiking neural network with direct input encoding and leakage and threshold optimization," *IEEE Transactions on Neural Networks and Learning Systems*, 2021.
- [13] S. Deng and S. Gu, "Optimal conversion of conventional artificial neural networks to spiking neural networks," in *International Conference on Learning Representations*, 2021. [Online]. Available: <https://openreview.net/forum?id=FZ1oTwcXchK>
- [14] T. Bu, W. Fang, J. Ding, P. DAI, Z. Yu, and T. Huang, "Optimal ANN-SNN conversion for high-accuracy and ultra-low-latency spiking neural networks," in *International Conference on Learning Representations*, 2022. [Online]. Available: https://openreview.net/forum?id=7B3IJMM1k_M
- [15] B. Han, G. Srinivasan, and K. Roy, "RMP-SNN: Residual membrane potential neuron for enabling deeper high-accuracy and low-latency spiking neural network," in *Proceedings of the IEEE/CVF Conference on Computer Vision and Pattern Recognition*, 2020, pp. 13 558–13 567.
- [16] Y. Wu, L. Deng, G. Li, J. Zhu, and L. Shi, "Spatio-temporal backpropagation for training high-performance spiking neural networks," *Frontiers in Neuroscience*, vol. 12, p. 331, 2018.
- [17] Y. Wu, L. Deng, G. Li, J. Zhu, Y. Xie, and L. Shi, "Direct training for spiking neural networks: Faster, larger, better," in *Proceedings of the AAAI conference on artificial intelligence*, vol. 33, 2019, pp. 1311–1318.
- [18] W. Fang, Z. Yu, Y. Chen, T. Huang, T. Masquelier, and Y. Tian, "Deep residual learning in spiking neural networks," *Advances in Neural Information Processing Systems*, vol. 34, pp. 21 056–21 069, 2021.
- [19] W. Fang, Z. Yu, Y. Chen, T. Masquelier, T. Huang, and Y. Tian, "Incorporating learnable membrane time constant to enhance learning of spiking neural networks," in *Proceedings of the IEEE/CVF International Conference on Computer Vision*, 2021, pp. 2661–2671.
- [20] B. Rueckauer, I.-A. Lungu, Y. Hu, M. Pfeiffer, and S.-C. Liu, "Conversion of continuous-valued deep networks to efficient event-driven networks for image classification," *Frontiers in Neuroscience*, vol. 11, p. 682, 2017.
- [21] P. U. Diehl, D. Neil, J. Binas, M. Cook, S.-C. Liu, and M. Pfeiffer, "Fast-classifying, high-accuracy spiking deep networks through weight and threshold balancing," in *2015 International joint conference on neural networks (IJCNN)*. IEEE, 2015, pp. 1–8.
- [22] D. Wu, X. Yi, and X. Huang, "A little energy goes a long way: Build an energy-efficient, accurate spiking neural network from convolutional neural network," *Frontiers in Neuroscience*, vol. 16, 2022.
- [23] N. Rathi, G. Srinivasan, P. Panda, and K. Roy, "Enabling deep spiking neural networks with hybrid conversion and spike timing dependent backpropagation," in *International Conference on Learning Representations*, 2020. [Online]. Available: <https://openreview.net/forum?id=B1xSperKvH>
- [24] J. Wu, C. Xu, X. Han, D. Zhou, M. Zhang, H. Li, and K. C. Tan, "Progressive tandem learning for pattern recognition with deep spiking neural networks," *IEEE Transactions on Pattern Analysis and Machine Intelligence*, 2021.
- [25] Y. Li, S. Deng, X. Dong, R. Gong, and S. Gu, "A free lunch from ann: Towards efficient, accurate spiking neural networks calibration," in *Proceedings of the 38th International Conference on Machine Learning*, ser. Proceedings of Machine Learning Research, M. Meila and T. Zhang, Eds., vol. 139. PMLR, 18–24 Jul 2021, pp. 6316–6325.
- [26] M. Yao, H. Gao, G. Zhao, D. Wang, Y. Lin, Z. Yang, and G. Li, "Temporal-wise attention spiking neural networks for event streams classification," in *Proceedings of the IEEE/CVF International Conference on Computer Vision*, 2021, pp. 10 221–10 230.
- [27] E. O. Neftci, H. Mostafa, and F. Zenke, "Surrogate gradient learning in spiking neural networks: Bringing the power of gradient-based optimization to spiking neural networks," *IEEE Signal Processing Magazine*, vol. 36, no. 6, pp. 51–63, 2019.
- [28] Y. Li, Y. Guo, S. Zhang, S. Deng, Y. Hai, and S. Gu, "Differentiable spike: Rethinking gradient-descent for training spiking neural networks," *Advances in Neural Information Processing Systems*, vol. 34, pp. 23 426–23 439, 2021.
- [29] Y. Kim and P. Panda, "Revisiting batch normalization for training low-latency deep spiking neural networks from scratch," *Frontiers in Neuroscience*, vol. 15, p. 773954, 2021.
- [30] C. Duan, J. Ding, S. Chen, Z. Yu, and T. Huang, "Temporal effective batch normalization in spiking neural networks," in *Advances in Neural Information Processing Systems*, A. H. Oh, A. Agarwal, D. Belgrave, and K. Cho, Eds., 2022. [Online]. Available: <https://openreview.net/forum?id=fLIggyQjIqz>
- [31] Z. Zhou, Y. Zhu, C. He, Y. Wang, S. YAN, Y. Tian, and L. Yuan, "Spikformer: When spiking neural network meets transformer," in *The Eleventh International Conference on Learning Representations*, 2023. [Online]. Available: https://openreview.net/forum?id=frE4fUwz_h
- [32] J. Zhang, B. Dong, H. Zhang, J. Ding, F. Heide, B. Yin, and X. Yang, "Spiking transformers for event-based single object tracking," in *Proceedings of the IEEE/CVF conference on Computer Vision and Pattern Recognition*, 2022, pp. 8801–8810.
- [33] Z. Wang, Y. Fang, J. Cao, Q. Zhang, Z. Wang, and R. Xu, "Masked spiking transformer," in *Proceedings of the IEEE/CVF International Conference on Computer Vision*, 2023, pp. 1761–1771.
- [34] Y. Li, T. Geller, Y. Kim, and P. Panda, "SEENN: Towards temporal spiking early-exit neural networks," *arXiv preprint arXiv:2304.01230*, 2023.
- [35] C. Li, E. Jones, and S. Furber, "Unleashing the potential of spiking neural networks by dynamic confidence," *arXiv preprint arXiv:2303.10276*, 2023.
- [36] J. Chen, S. Park, and O. Simeone, "Agreeing to stop: Reliable latency-adaptive decision making via ensembles of spiking neural networks," *arXiv preprint arXiv:2310.16675*, 2023.
- [37] G. Shafer and V. Vovk, "A tutorial on conformal prediction." *Journal of Machine Learning Research*, vol. 9, no. 3, 2008.
- [38] B. Rückauer, N. Känzig, S.-C. Liu, T. Delbruck, and Y. Sandamirskaya, "Closing the accuracy gap in an event-based visual recognition task," *arXiv preprint arXiv:1906.08859*, 2019.
- [39] S. Deng, Y. Li, S. Zhang, and S. Gu, "Temporal efficient training of spiking neural network via gradient re-weighting," in *International Conference on Learning Representations*, 2022. [Online]. Available: https://openreview.net/forum?id=_XNtisL32jv
- [40] R. Banner, I. Hubara, E. Hoffer, and D. Soudry, "Scalable methods for 8-bit training of neural networks," *Advances in Neural Information Processing Systems*, vol. 31, 2018.

- [41] G. Biau and D. M. Mason, “High-dimensional p p -norms,” in *Mathematical statistics and limit theorems*. Springer, 2015, pp. 21–40.
- [42] K. He, X. Zhang, S. Ren, and J. Sun, “Deep residual learning for image recognition,” in *Proceedings of the IEEE Conference on Computer Vision and Pattern Recognition*, 2016, pp. 770–778.
- [43] A. Krizhevsky, G. Hinton, *et al.*, “Learning multiple layers of features from tiny images,” *Toronto, ON, Canada*, 2009.
- [44] Y. Le and X. Yang, “Tiny imagenet visual recognition challenge,” *CS 231N*, vol. 7, no. 7, p. 3, 2015.
- [45] H. Li, H. Liu, X. Ji, G. Li, and L. Shi, “Cifar10-DVS: an event-stream dataset for object classification,” *Frontiers in Neuroscience*, vol. 11, p. 309, 2017.
- [46] G. Orchard, A. Jayawant, G. K. Cohen, and N. Thakor, “Converting static image datasets to spiking neuromorphic datasets using saccades,” *Frontiers in Neuroscience*, vol. 9, p. 437, 2015.
- [47] S. B. Shrestha and G. Orchard, “Slayer: Spike layer error reassignment in time,” *Advances in Neural Information Processing Systems*, vol. 31, 2018.
- [48] E. D. Cubuk, B. Zoph, D. Mane, V. Vasudevan, and Q. V. Le, “Autoaugment: Learning augmentation strategies from data,” in *Proceedings of the IEEE/CVF Conference on Computer Vision and Pattern Recognition*, 2019, pp. 113–123.
- [49] N. Srivastava, G. Hinton, A. Krizhevsky, I. Sutskever, and R. Salakhutdinov, “Dropout: a simple way to prevent neural networks from overfitting,” *The journal of machine learning research*, vol. 15, no. 1, pp. 1929–1958, 2014.
- [50] G. Jin, X. Yi, P. Yang, L. Zhang, S. Schewe, and X. Huang, “Weight expansion: A new perspective on dropout and generalization,” *Transactions on Machine Learning Research*, 2022.

APPENDIX

APPENDIX A

INEQUATION PROOF

We follow [40] to derive the bound of expected norm of a random variable vector. By Jensen’s inequality, it gives

$$\begin{aligned} \mathbb{E}(\|\mathbf{V}(t)\|_2) &= \mathbb{E}\left(\sqrt{\sum_i V_i(t)^2}\right) \leq \sqrt{\mathbb{E}\left(\sum_i V_i(t)^2\right)} \\ &= \sqrt{\sum_i \mathbb{E}(V_i(t)^2)} \end{aligned} \quad (1)$$

As the $V_i(t)$ is a uniform random variable in range $[0, V_{\text{thr}}]$, the expected value of $V_i^2(t)$ can be computed as follows

$$\mathbb{E}(V_i^2(t)) = \int_0^{V_{\text{thr}}} x^2 \frac{1}{V_{\text{thr}}} dx = \frac{V_{\text{thr}}^2}{3} \quad (2)$$

which yields

$$\mathbb{E}(\|\mathbf{V}(t)\|_2) \leq \frac{\sqrt{n}V_{\text{thr}}}{\sqrt{3}} \quad (3)$$

Since t and S_r are constant values, the following inequality holds

$$\mathbb{E}(\|\mathbf{V}(t)/(tS_r)\|_2) \leq \frac{\sqrt{n}V_{\text{thr}}}{\sqrt{3}tS_r} \quad (4)$$